89
10-31-79

Lib. 209

LA-8048-MS, Vol. I

Informal Report

Aguila Pre-Operations Plan

University of California

LOS ALAMOS SCIENTIFIC LABORATORY

Post Office Box 1663 Los Alamos, New Mexico 87545

LA-8048-MS, Vol. I
Informal Report

UC-34b
Issued: September 1979

Aguila Pre-Operations Plan

David Simons
Morris Pongratz
Melvin Duran
Guy Barasch

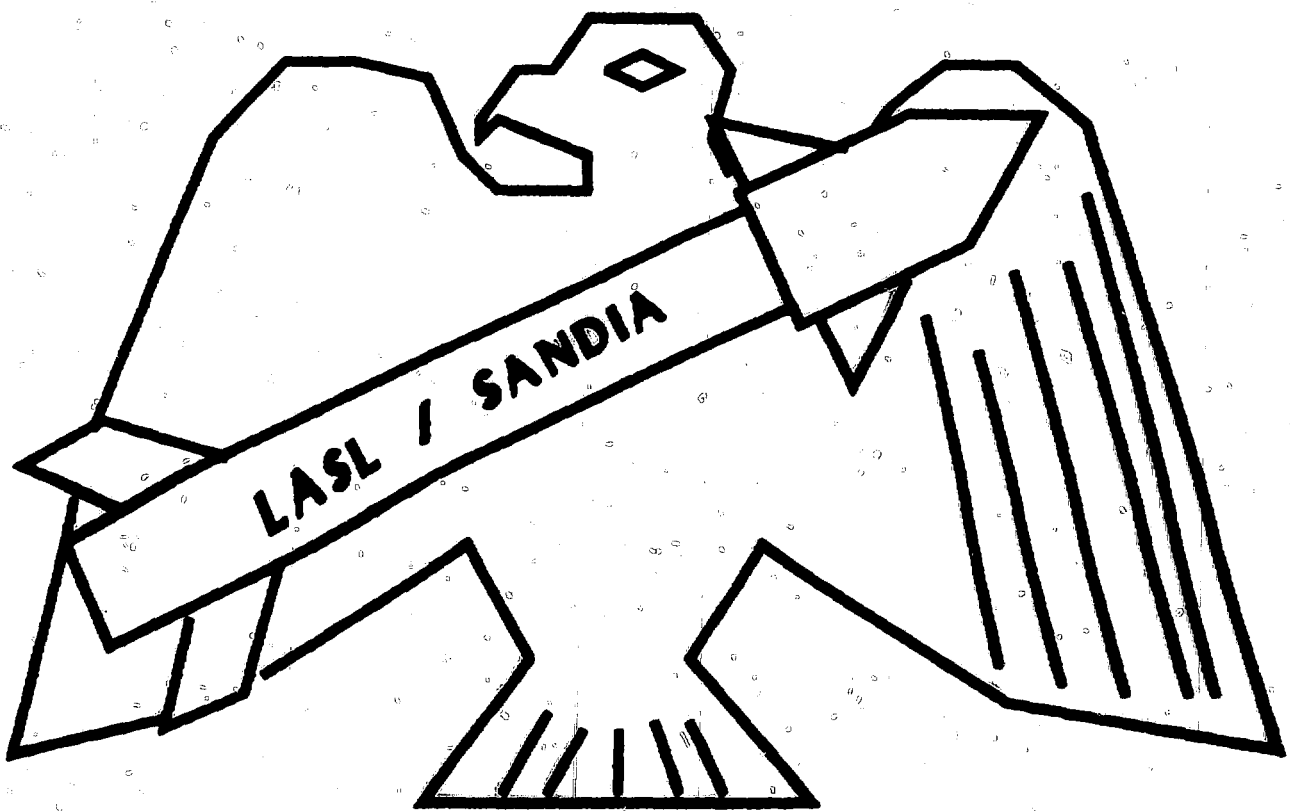

AGUILA PRE-OPERATIONS PLAN

by

David Simons, Morris Pongratz, Melvin Duran, and Guy Barasch

ABSTRACT

Aguila, a small-rocket experiment addressing the structuring of ionospheric plasmas, is described. A Terrier-Malemute two-stage rocket will be launched approximately north from Kauai Test Facility after sunset between October 8 and October 21, 1979, universal time. Aguila will deposit three barium clouds: before apogee at about 360 and 520 km, and just after apogee at 560 km. These clouds will be photoionized by the sun and observed using intensified-camera and television systems and photometers that are sensitive to barium line radiations. These observations will be made from ground stations on Mt. Haleakala, Maui, and at the launch site. Each cloud's striation time and subsequent behavior will elucidate mechanisms believed to drive ionospheric-plasma morphology.

INTRODUCTION

Operation Aguila (Eagle), a single-rocket barium-release experiment being conducted jointly by LASL and SLA, will study what may be the dominant mechanism in prompt structuring of upper-atmospheric plasmas (striations) produced by high-altitude nuclear bursts. Striated plasmas degrade radio propagation between surface or airborne terminals and satellite-borne communications links; depending on rf frequency, the degradations can be wide-spread and long-lasting. A quantitative description of the formation, evolution, and decay of nuclear-explosion-induced striations is a fundamental prerequisite for the performance evaluation of both existing and future satellite-to-ground communications command, control, and intelligence (C^3I) links.

During Fishbowl, the 1962 series of high-altitude nuclear tests, the nuclear-induced plasmas striated within a short time after the detonations. Since 1962, only LASL's shaped-charge barium experiments and the CAMEO series have succeeded in forming prompt striations in the ionosphere. Our theoretical research strongly suggests that these striations simulate high-altitude nuclear-explosion-induced striations. In spite of the empirical evidence, relatively little research has been devoted to a theoretical explanation of prompt structure, and the effects of prompt structure on communications systems have not been extensively evaluated. Consequently, descriptions of prompt striations and their effects have not been available to satellite-communications-equipment designers.

The early-time effects of nuclear-induced plasmas over the UHF spectrum are so severe that details of the plasma behavior during the first few minutes following a burst have been of little concern to the satellite-system community. Also, it has not been widely appreciated that formation of prompt striations at high altitudes accelerates the entire process of formation of plasma structure and its final decay, which changes the space-time volume substantially.

New satellite communications systems are being planned and implemented. They will require more extensive knowledge than now exists regarding early striation formation and subsequent evolution. These communications systems differ from present ones in that they will use higher frequencies and will have modulation/demodulation schemes designed to mitigate against nuclear effects. These differences reduce degradations by nuclear plasmas, thereby reducing the volume and duration over which communications degradations are induced. The reduced duration of effects places great significance on early plasma structure and its evolution.

Prompt striation formation in ionospheric plasma clouds apparently results from a peaked distribution in the component of ion velocity perpendicular to the geomagnetic field. In the nuclear case, debris ions large distances from the burst have highly peaked velocity distributions, which excite instabilities. Only barium releases with a peaked perpendicular velocity distribution have been observed to form prompt striations. These releases include all the LASL shaped-charge experiments that were released with a significant perpendicular velocity component. Prompt striations also occurred in the thermite-

release experiment, CAMEO (conducted by NASA), where the release velocity included an orbital vehicle velocity of 7 km/s perpendicular to the geomagnetic field.

Thermite releases conducted near apogee in small-rocket experiments are thought not to form prompt striations, but to striate slowly by the gradient drift instability. This is surely true for release altitudes below 300 km, where the high rate of collisions promptly thermalizes any directed ion velocities. Previously, thermite releases (other than CAMEO) conducted above 300 km, where collisions are relatively unimportant, have not been diagnosed adequately to detect prompt striations, if present. It was inferred indirectly that prompt striations occurred on the NASA-MPE barium release at 5 R_E.[1]

The prompt striations that appear in ionospheric plasmas having peaked perpendicular-velocity distributions are predicted by Simons and Pongratz to arise from saturation of a linear plasma instability called the drift cyclotron loss cone (DCLC). The linear DCLC theory predicts high instability growth rates corresponding to the prompt onset of striations for the nuclear case, perpendicular shaped-charge barium experiments, and CAMEO. The linear theory also predicts that the onset of prompt striation production should occur for certain thermite releases above 300 km if additional vehicle velocities perpendicular to the field from 1 to 2 km/s are present. Such releases would be equivalent to CAMEO, but at suborbital velocities.

Aguila's primary objective is to test these DCLC theory predictions by optically investigating prompt striation production for three barium-thermite releases from a moving vehicle. Perpendicular velocities for two of the releases will be in the range of 1 to 2 km/s, where DCLC onset is predicted; one release will be conducted at a low vehicle velocity. The measured striation onset times will be compared to DCLC predictions; these times can be contrasted with predictions by gradient-drift instability theory for the Aguila cloud parameters. A summary of DCLC theory and its application to the Aguila clouds are given in the Appendix.

The DCLC theory also predicts enhanced production of suprathermal electrons, leading to enhanced oxygen airglow emission. Therefore, Aguila observations will include airglow measurements.

The parameters characterizing the plasma during the linear DCLC instability do not necessarily characterize the plasma as the instability approaches saturation. It is in the near-saturation regime that the macroscopic structure actually evolves in the plasma. The evolution of the plasma cloud is

ultimately controlled by properties of the system such as total available energy, wave and particle convection, and turbulence saturation. These properties cannot be included in a linear theory. Aguila has been designed to study the formation of prompt structure specifically in terms of the physical parameters describing the linear DCLC theory. By diagnosing striation onset time, initial structure size, and extent of electron heating as a function of initial cloud parameters and structure size, we will extend our understanding into the area of nonlinear development.

Once striated, the Aguila clouds may: evolve to finer structure via gradient drift; "freeze in" at some stage of development; or, if the neutral wind coupling to the clouds is very weak, diffuse away. We will follow the later-time evolution of the ion clouds as a secondary objective.

EXPERIMENT

Rocket Trajectory

In cooperation with Sandia and Thiokol, we are designing a rocket payload that will be carried aboard a Terrier-Malemute sounding rocket to be launched from the Kauai Test Facility. The rocket will fly north close to the magnetic meridian and will deploy three barium-ion clouds via thermite injection (cupric-oxide/barium thermite). The clouds will be deployed at approximately 350-, 520-, and 560-km altitude, respectively. These injection altitudes are high enough to ensure essentially collision-free evolution of the plasma clouds. The velocity of the rocket transverse to the magnetic field will be different for each of the three injections. Each cloud falls into a different portion of the DCLC linear-parameter regime and has a considerably different amount of free energy available to feed this instability. The cloud at 350 km has the highest perpendicular velocity, is the most unstable, and should structure most rapidly. The cloud at 520 km has an intermediate velocity, is somewhat less stable, and should require a longer time to striate. The cloud at 560 km has a very small perpendicular velocity, is only marginally unstable, and probably will not form any prompt structure. This cloud may eventually striate by 'gradient drift,' but on a much longer time scale (on the order of many hours).

In Fig. 1, we show a sample trajectory for the Terrier-Malemute projected into a north-vertical plane. The three injections with their times relative to lift-off are indicated. Although the final trajectory may differ somewhat as a result of further calculations, Fig. 1 will represent our model trajectory for all the calculations contained in this report. Very similar results have been obtained using a variety of like trajectories, so we do not anticipate any radical departures from the predictions discussed here.

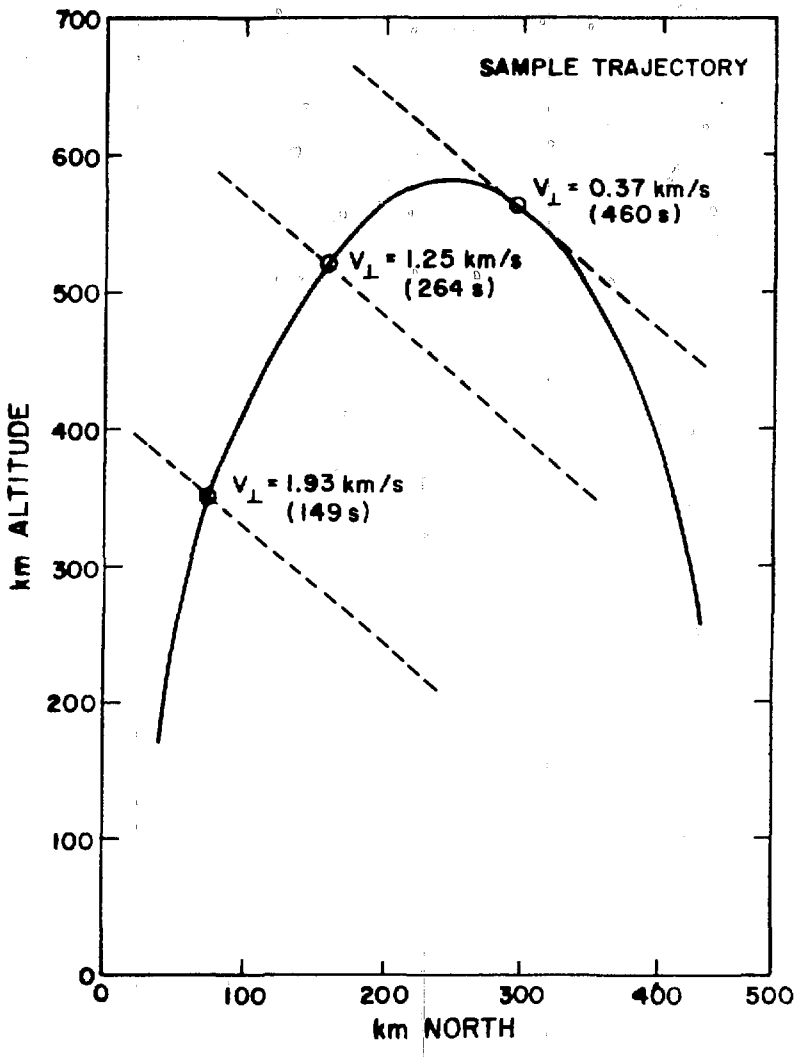

Fig. 1.
Terrier-Malemute trajectory showing the three release points.

Barium-Thermite Payload

The payload stage of the Terrier-Malemute rocket will be 16" in diameter and 18" in length, housing three cylindrical thermite canisters. Each canister will have one 120^{o} nozzle pointing radially outward, spaced at 120^{o} intervals around the circumference of the payload. The characteristics of the thermite injection were provided to us in discussions with G. Alford of Thiokol and J. Heppner of NASA/Goddard, a NASA document,[2] and an article by K. W. Michel.[3]

The barium-thermite canister contains cupric-oxide, barium metal, and argon gas. The temperature in the vessel reaches about 3200 K at slightly less than 700-psi pressure. Microparticles of barium metal, BaO, copper, and argon are expelled from the nozzle as a mist. These particles evaporate rapidly, leading to rapidly cooling microparticles and an expanding gas of atomic barium. During the fraction of a second that the process is collision-dominated, directed energy is imparted to the neutral barium gas, resulting in a 180^{o} expanding shell of barium atoms. The shell has a velocity of about 1 km/s and a velocity spread of about 0.5 km/s. This velocity distribution is well-represented by

$$f(v) \propto v^2 \exp\left[-\frac{(v - v_o^2)}{2v_T^2}\right] , \qquad (1)$$

where v_o = 1 km/s and v_T = 0.5 km/s. Haerendel et al[4] discuss the physics of the formation of this shell.

The canisters, containing 8 kg of barium metal, require about 1 to 1.5 s to exhaust the barium vapor completely. During this time, the payload section will rotate at least 5 times. The combined effect of the rotation and the exhaust period will lead to a nearly isotropic neutral barium shell-like cloud expanding around the rocket's center of mass motion. Because the thermite process is about 8% efficient, each cloud will initially contain some 2.8×10^{24} barium atoms.

Velocity Distribution

The low injection velocity of barium vapor resulting from thermite injection will enable us to vary the total injection velocity of three barium

clouds over a range appropriate to the testing of the DCLC prompt striation mechanism. LASL has employed thermite injection in the past,[5] but we add controlled use of the vehicle velocity in Aguila to obtain three different cross-field injection velocities. This will extend the investigation of prompt striations into the threshold-velocity region of 1-km/s injection velocities.

Optical Diagnostics

The barium clouds will be optically diagnosed from two ground stations: a primary station located on top of Mt. Haleakala, and a smaller station located at the Barnyard in Kauai. Because all three barium clouds will be spatially separated when viewed from Mt. Haleakala, this station will be the most heavily instrumented. Figure 2 is a theoretical determination of the spatial extent of the barium clouds at a time 30-s after the release of the third

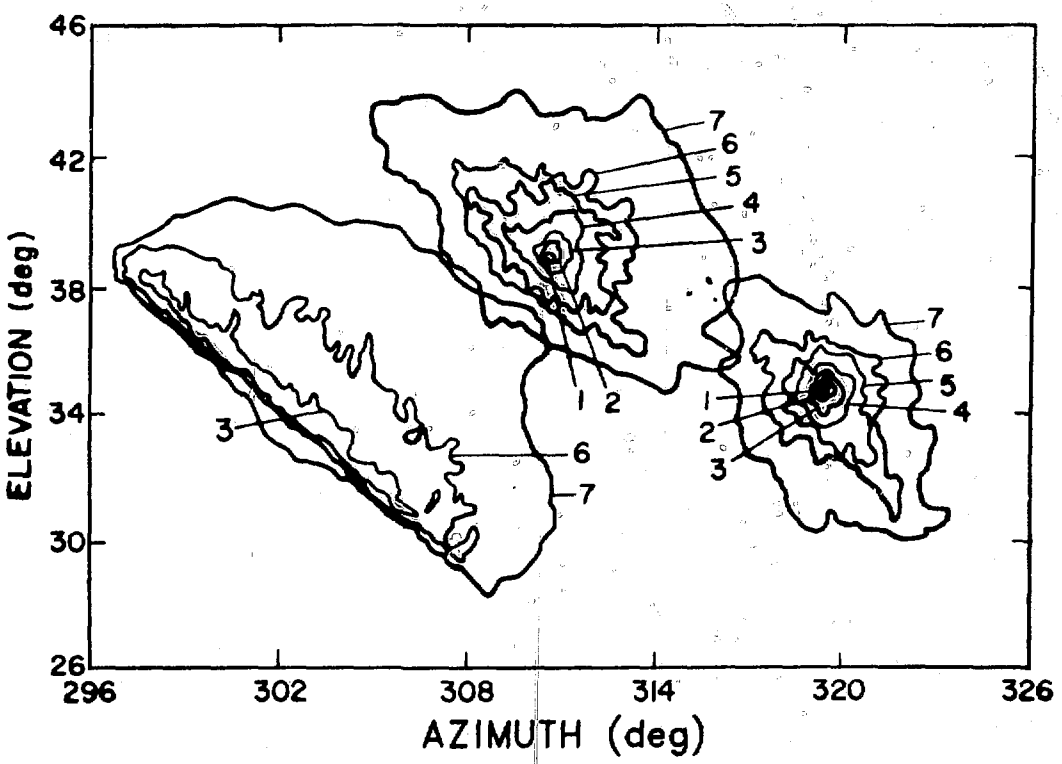

Fig. 2.
Iso-column-density contours of the three events viewed from Haleakala Station at Event III plus 30 seconds in particles/cm^2: 1 = 10^{12}, 2 = 5 x 10^{11}, 3 = 10^{11}, 4 = 5 x 10^{10}, 5 = 10^{10}, 6 = 5 x 10^9, and 7 = 10^9.

event. It is a display of the integrated line-of-sight column density of barium ions as seen from Mt. Haleakala. All three events are adequately separated in the field of view. The small station at the Kauai Barnyard will provide auxiliary views of the clouds, with considerable obstruction of Clouds II and III by Cloud I.

Both stations will be instrumented to determine: (1) the neutral barium velocity distribution, (2) the distribution and structure of barium ions, (3) the spatial extent and degree of electron heating, and (4) neutral winds. The instrumentation will chiefly consist of intensified cameras filtered for neutral- and ionized-barium resonance fluorescence and for airglow from the excited ground states of oxygen. The film cameras will be supplemented by intensified television cameras (for pointing and documentation) and photometers.

The Maui station instrument plan is given as Table I. Three trackers are specified, each mounting narrow-field instruments to be pointed at one cloud at a time. All trackers will be pointed at the first event; two of them will subsequently be moved to record Event Two; and two of them will again be moved to record Event III. The schedule of these moves is given in Table II. In addition to the three trackers, there will be one fixed mount containing wide-field instrumentation for backup multi-cloud recording.

The Kauai station instrument plan is given in Table III. One tracker will carry the narrow-field instrumentation and will be pointed toward each of the three events in turn. Primary emphasis will be placed on Event I since Events II and III will be partially obscured by the Event-I ion cloud.

Launch Window

These requirements will determine launch time: evening, solar depression angle, and a moonless sky.

Evening - The requirement for Aguila to be an evening launch derives from our fundamental need to distinguish between DCLC-driven striations and gradient-drift driven striations. This distinction will be based on time-to-onset of the striations. DCLC is fast; therefore we must choose conditions that will slow gradient-drift striation formation. Gradient-drift formation will be slower in the evening (when Pederson conductivities of the ionosphere are relatively high) than in the morning.

TABLE I

INSTRUMENT PLAN

CAMERA*		INTENS.	FILTER		LENS				Exposure	FILM					CAMERA
Type	S/N	(***)S/N	λ	S/N	F.L.	Aper.	F.O.V.	S/N	Seq.	Type	Emul.	Size	Length	Perf.	Position
					(mm)		(H/V)		No.		No.	(mm)	(ft)	No.	**
-ISIT	1	---	4554	5-75-2	15-120	1.3	6.1/4.6 46/35	730444		VIDEO TAPE					T-1
MICA	802	2	5854		2500	14				TRI-X		35	100		T-1
ICA	804	128601	6142		400	1.8	5/3.6	6-062		TRI-X		35	100		T-1
CA	500	---	4554	3-75-8	150	1.8				TRI-X		35	100		T-1
ISIT	2	---	4554	5-75-3	15-120	1.3	6.1/4.6 46/35	730225		VIDEO TAPE					T-2
MICA	801	1	5854		2500	14				TRI-X		35	100		T-2
ICA	808	1211	6142		400	1.8	5/3.6	6-065		TRI-X		35	100		T-2
ICA	501	126603	4554	4-72-3	150	1.8	13/9.5	70755		TRI-X		35	100		T-2

EXPOSURE SEQUENCE

No.	Start Time	Exposure	No.	Start Time	Exposure

NOTES

*Unless otherwise noted, all camera systems record universal time.

**Indicate with an arrow the orientation of the data chamber.

***Indicate the phosphor color, B=blue, G=green.

Prepared by

Date 7/24/79

Station Maui

Event Aquila

Event Date

TABLE I (continued)

INSTRUMENT PLAN

CAMERA*		INTENS.	FILTER		LENS				Exposure	FILM					CAMERA
Type	S/N	(***)S/N	λ	S/N	F.L.	Aper.	F.O.V.	S/N	Seq.	Type	Emul.	Size	Length	Perf.	Position
					(mm)		(H/V)		No.		No.	(mm)	(ft)	No.	**
-IO	1	---	4554	4-72-1	150-300	4.5				VIDEO TAPE					T-3
MICA	803	3	5854		1250	10	1.6/1.2	277222		TRI-X		35	100		T-3
ICA	805	6608	5854	6"	203	1.5	9.8/7	2141		TRI-X		35	100		T-3
ICA	502	1507	5535		150	1.8	13/9.5	67113		TRI-X		35	100		T-3
ICA	503	791	6300	4-75-3	76	0.87	25/18	451		TRI-X		35	100		T-3
Photo-meter	Tilt		(1)		---					VISICORDER FM RECORDER					T-3
IO	2	---	4554	6-72-1	105	0.75				VIDEO TAPE					GORDON
ICA	504	1388	6142		50					TRI-X			100		GORDON
ICA	505	8600	5535	5558 1-68	50	0.95	35/27	100688		TRI-X			100		GORDON
ICA	806	8603	6300		50	0.95	35/27	104584		TRI-X			100		GORDON
CA	506	---	5535	5558 3-68	50	0.95	35/27	25472		TRI-X			100		GORDON
CA	507	---	4554	3-75-6	50	0.95	35/27	259-51		TRI-X			100		GORDON
Canon (F1)		---	---		50	1.4				Kodacolor 400		35	36 exp.		GORDON

EXPOSURE SEQUENCE

No.	Start Time	Exposure	No.	Start Time	Exposure

NOTES

(1) 6300#, 5577#, 5754#

*Unless otherwise noted, all camera systems record universal time.

**Indicate with an arrow the orientation of the data chamber.

***Indicate the phosphor color, B=blue, G=green.

Prepared by

Date 7/24/79

Station Maui

Event Aquila

Event Date

TABLE II

PRELIMINARY TRACKING PLAN - MAUI

	Event I	Event II	Event III
Tracker I	0-430,590-∞	---	450-570
Tracker II	0-230	250-∞	---
Tracker III	0-230	250-430	450-∞

(Times after lift-off)
Event I is 149 s after liftoff
Event II is 264 s after liftoff
Event III is 460 s after liftoff

Gradient drift growth rates for the Aguila cloud parameters are derived as follows: The linear theory of the gradient drift instability at high altitudes yields the relationship[6,7]

$$\gamma_{GD} = \frac{\left(\frac{\varepsilon cE}{B}\nu_{in}\right)^{1/2}}{1 + \frac{\Sigma_{PB}}{\Sigma_{PC}}}, \qquad (2)$$

where γ_{GD} is the linear growth rate, ν_{in} is the ion neutral-collision frequency, ε is the inverse gradient scale length, cE/B is the neutral wind velocity, and $(\Sigma_{PB}/\Sigma_{PC})$ is the ratio of the integrated background Pedersen conductivity to the integrated cloud conductivity. At sunset, the integrated ionospheric Pedersen conductivity is about 9×10^{11} electrostatic units, while at sunrise it is about 3×10^{10}. This is a factor of 30 difference in the ratio of integrated conductivity. Other gradient drift parameters are given in Table IV.

To be conservative, we assume a large neutral wind velocity of 200 m/s. Table V gives the resulting gradient-drift growth rates, γ_{GD}, for evening and morning ionospheres. The lowest event would require 3 to 6 minutes to striate in the morning, but will require from 40 minutes to more than an hour in the evening. The evening window is clearly superior for this event. It is of no

TABLE III

INSTRUMENT PLAN

CAMERA*		INTENS.	FILTER		LENS				Exposure	FILM					CAMERA
Type	S/N	(***)S/N	λ	S/N	F.L.	Aper.	F.O.V.	S/N	Seq.	Type	Emul.	Size	Length	Perf.	Position
					(mm)		(H/V)		No.		No.	(mm)	(ft)	No.	**
ISIT	RCA	---	4554	3-75-12	RCA ZOOM					VIDEO TAPE					Elephant
ICA	800	1174	6142		400	1.8	5/3.6	6-066		TRI-X		35	100		Elephant
ICA	*508*	*1457*	(1)		50	0.95	*35/27*			*TRI-X*		*35*	*100*		*Elephant*
CA	509		4554	3-75-11	50	0.95	35/27	26033		TRI-X		35	100		Elephant
Canon (E1)					50	1.4	35/27	718667		Kodacolor 400		35	36 exp.		Elephant
Photo-meter	Prit-chard														Elephant
Canon (IE1)			(2)		50	1.4				TRI-X		35	250 exp.		Elephant

EXPOSURE SEQUENCE

No.	Start Time	Exposure	No.	Start Time	Exposure

NOTES

(1) 5535# 25 Å, Not num., 4554# 3-75-5

(2) 5535# 2, 4554# 3-75-7

*Unless otherwise noted, all camera systems record universal time.

**Indicate with an arrow the orientation of the data chamber.

***Indicate the phosphor color, B=blue, G=green.

Prepared by

Date 7/24/79

Station Kauai

Event Aguila

Event Date

TABLE IV

G-D PARAMETERS

	ν_{in}	ϵ, per km	Σ_{PC}
Event I	3.5×10^{-2}	1.7×10^{-2}	3.63×10^{10}
Event II	3.3×10^{-3}	2.2×10^{-2}	2.26×10^{9}
Event III	2.0×10^{-3}	3.6×10^{-2}	1.45×10^{9}

great advantage for Events II and III because the striation times in both morning and evening are sufficiently long.

It has been suggested that, rather than the neutral wind velocity, one should use the injection velocity, v_o, in Eq. (2) to calculate the growth rate. Taking 3 km/s for Event I yields a growth time of 10 minutes in the evening ionosphere; however, this would require that the fast neutral barium be present for 10 minutes to provide this effective neutral wind, whereas essentially all the fast neutral barium is gone within one minute. Under these circumstances, we feel the (background) neutral wind velocity is the appropriate parameter in Eq. (2).

Solar depression angle - The sun must be high enough that the events will be illuminated by solar ultraviolet, but low enough that the sky brightness is quite small at event time.

TABLE V

G-D GROWTH RATES

	Evening	Morning
Event I	4.2×10^{-4}/s	6.0×10^{-3}/s
Event II	9.5×10^{-6}/s	2.7×10^{-4}/s
Event III	6.1×10^{-6}/s	1.8×10^{-4}/s

According to Pongratz and Jeffries,[8] the altitude of the UV terminator is ~ 40 km above the altitude of the visible terminator, and the altitude of the visible terminator may be well-approximated by H_V (km) = [α (degrees)]^2, where H_V is the visible terminator altitude and α is the solar depression angle. The Event-I altitude, 360 km, will therefore be illuminated until the solar-depression angle reaches 18°.

The sky brightness is sufficiently low by 12° solar-depression angle to permit good observation at all lines in the visible. Figure 3 gives a value of 10^{-11} W/cm^{2}sr nm at 455.4 nm.[9] We therefore choose to execute Event I at a time when the solar depression angle is not less than 12°.

The Event-I ion cloud (360 km) will sink due to gravity, even while the visible terminator is rising. Thus, Event I will probably be observable for only 20 minutes. To keep from shortening Event-I observation time very drastically, we will not launch more than 10 minutes after the earliest launch time given above. Therefore, the launch window for each night will be 10-minutes long.

Event III (560 km) will also sink due to gravity, but because of its higher altitude, it will be observable until about 20° solar depression angle.

Moonless Sky - The moon must be below the horizon for solar-depression angles between 12 and 20°, due to the previous requirements. From Fig. 4, a plot of moon rise and set times vs date, we can define the dates during October with satisfactory lunar conditions.

The first day in October that moon-rise is after 24° solar-depression angle is October 8 (UT). Note that October 8 (UT) represents Sunday evening, October 7, local time. We are considering an automatic 24-hr delay to avoid the holiday. The last day in October that the moon sets prior to 12° solar-depression angle is October 21 (UT).

OPERATIONS

Personnel

Aguila personnel and their tasks are summarized in Fig. 5.

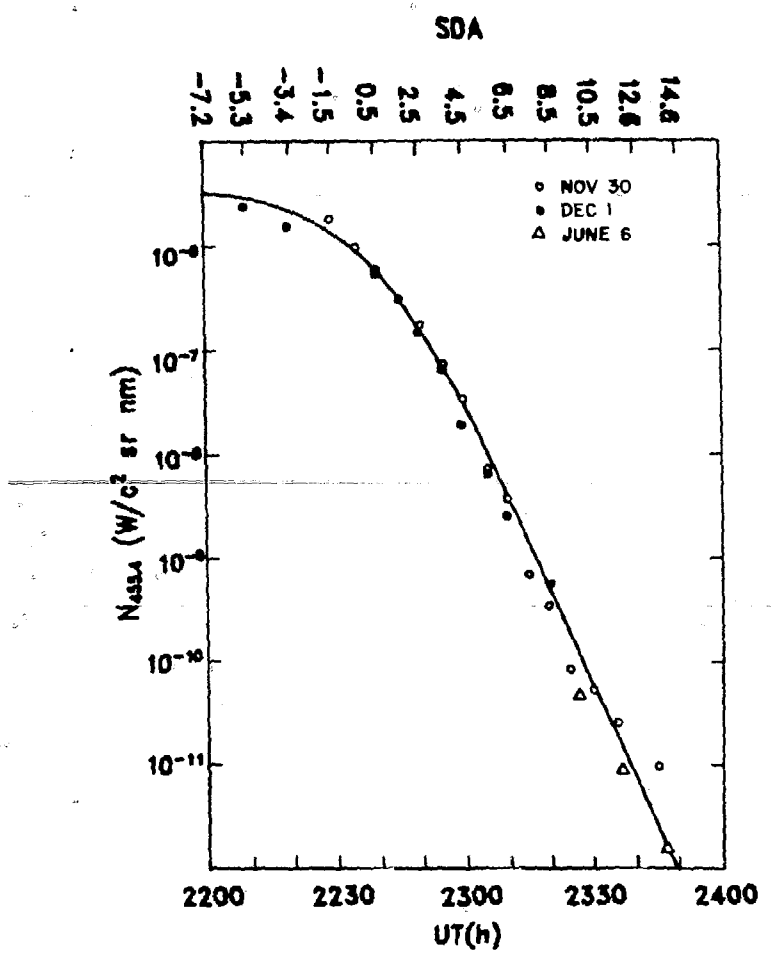

Fig. 3.
Sky brightness at 455.4 nm as a function of solar depression angle.[9]

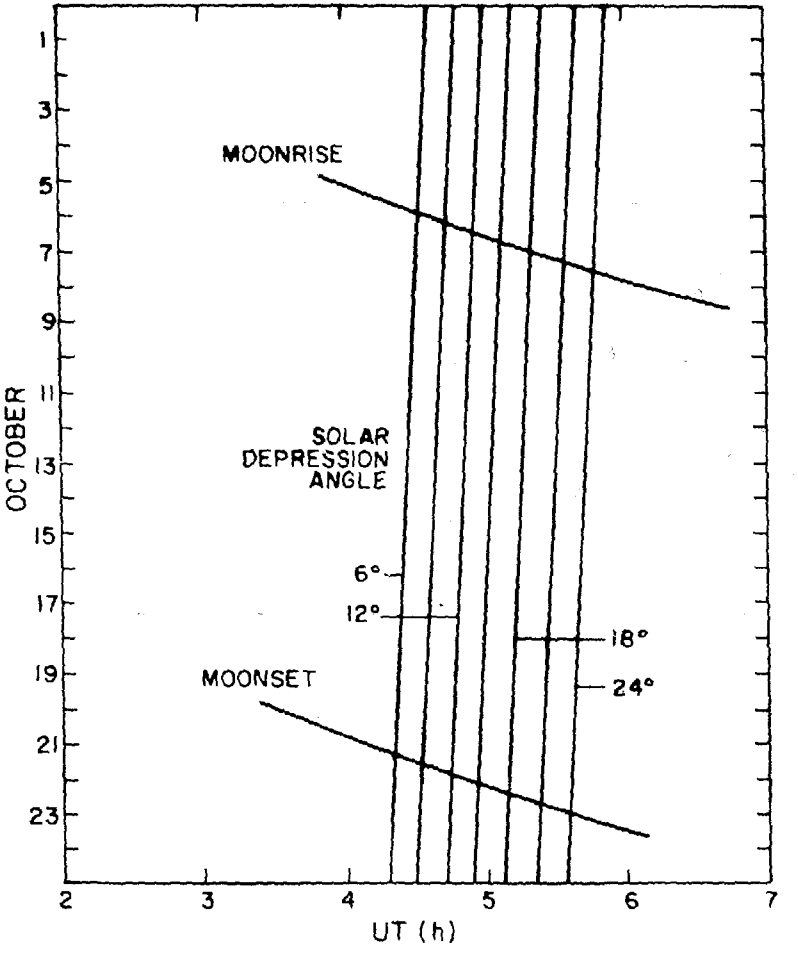

Fig. 4.
Moonrise and moonset versus solar depression angle from Mt. Haleakala.

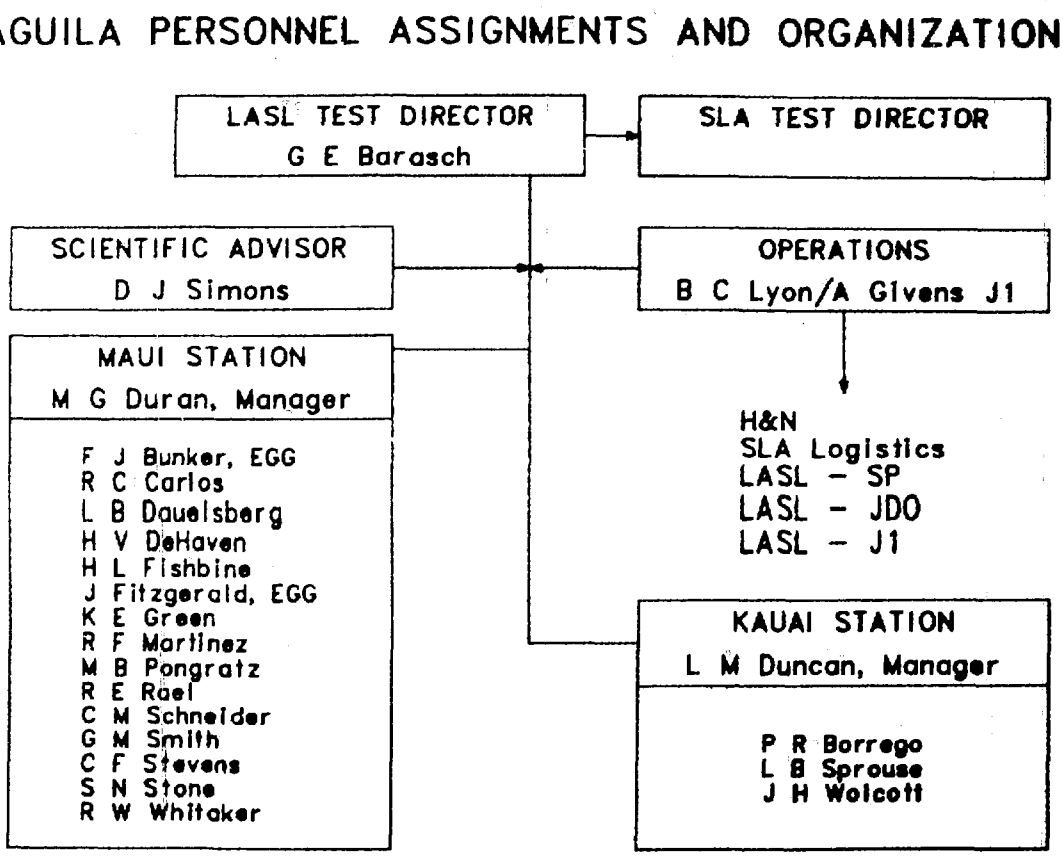

Fig. 5.

Schedule

Aguila will be prepared for field readiness for the launch window of October 8 through 21, 1979 (universal time; corresponds to the evenings of October 7 through 20, 1979, Kauai local time). To achieve readiness, LASL personnel will deploy by September 24, 1979. The LASL Test Director will reach Kauai by September 20. Other dates are summarized in the Aguila schedule of Fig. 6. Of particular importance are the dry-run weeks, August 13 through 17 (Los Alamos) and October 1 through 6 (in the field). These exercises are essential to develop facility with the complex equipment and tracker repointing.

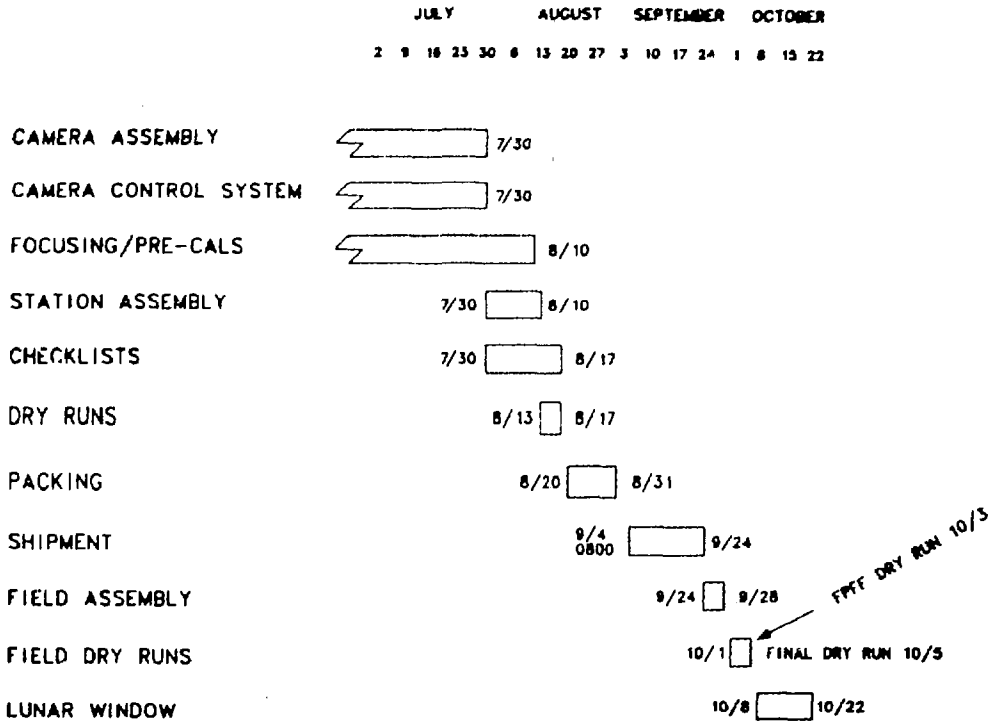

Fig. 6.

Communications

The communications plan is summarized in Fig. 7. Two nets are of primary importance: the hard-wire net from Aguila control, KTF, to Maui; and the event-point predictor telephone line to Maui.

Logistics Support

Logistics support is presently being handled by J-1. Requests for in-the-field support by Sandia and Holmes and Narver will be made through DoE/PASO.

Weather Information

LASL will operate a satellite-picture weather receiver somewhere at PMR/KTF. LASL will also consult daily with NOAA/Honolulu weather experts. Plans are being firmed up jointly (J-1, LASL; Canute, SLA).

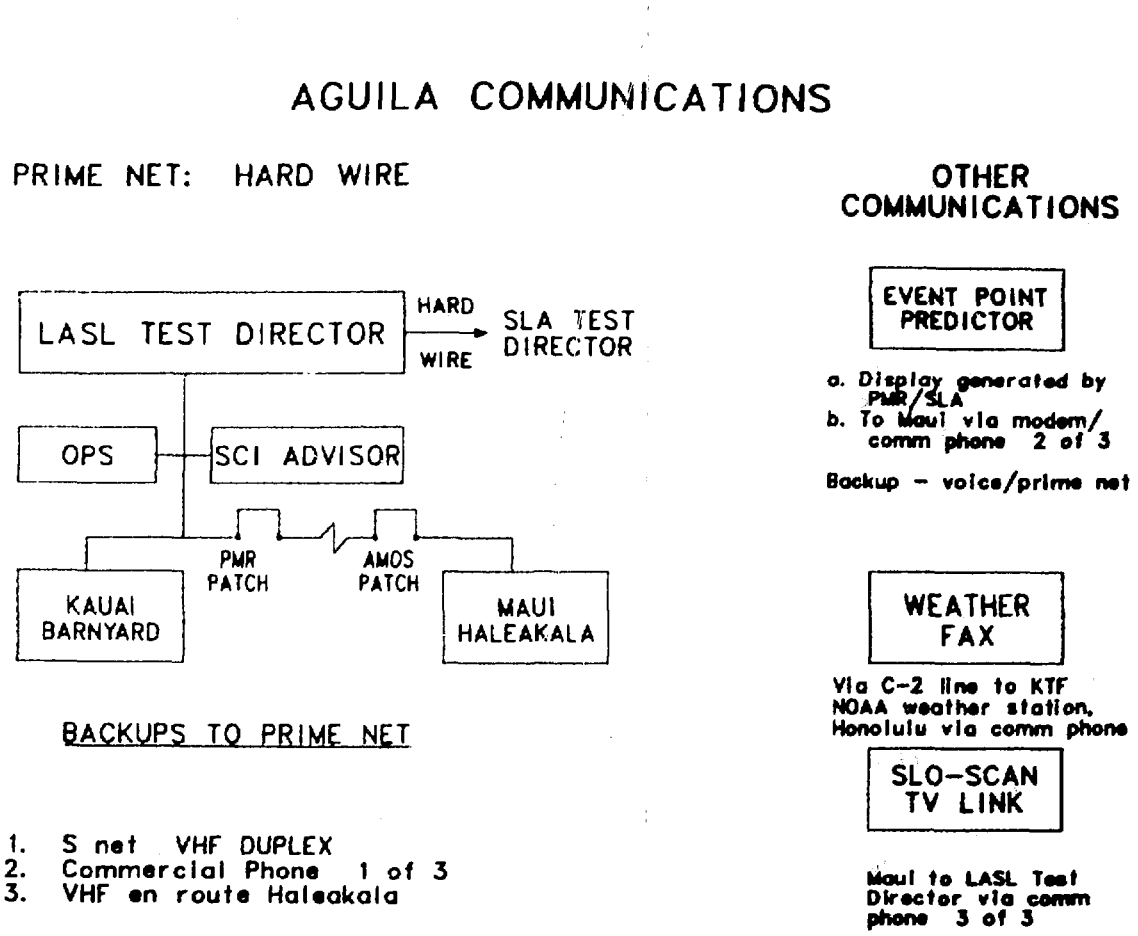

Fig. 7.

ACKNOWLEDGMENTS

We gratefully acknowledge the efforts of our colleagues at Sandia Laboratories, Albuquerque; in particular Bill Barton, Dick Eno, Al Huters, Ted Krein, and Bill Millard, in making many aspects of this experiment possible. We thank John Davis and his associates at Pacific Missile Range, Oxnard, CA, for their part in the all-important event-point-prediction capability, and we are grateful to Jim Newell, J-DO, for helping us arrange the transmittal of the information to our stations. We are indebted to the J-10 field-experimental team who are bringing this plan to fruition. Unswerving support and guidance from Bob Jeffries, J-DO, are also gratefully acknowledged.

APPENDIX

THE DCLC THEORY

The DCLC theory is central to the conceptualization of Aguila. We will, therefore, provide a fairly detailed presentation in this Appendix. A complete description of the theory is contained in papers by Simons and Pongratz[10] and Simons et al.[11] We will discuss each parameter that characterizes the linear instability and explain its physical significances. In addition, we will introduce two parameters that may characterize the nonlinear evolution of the DCLC instability.

The theory assumes that an anisotropic, low-β plasma is initially confined in a magnetic field. This plasma has spatial density gradients and the specific anisotropy is a peak in the perpendicular velocity distribution resulting from cross-field injection of neutral barium atoms that photoionize and become trapped in the magnetic field. The density gradient is characterized by a local density scale length, ε_α, defined by

$$\varepsilon_\alpha = \frac{1}{\eta_\alpha} \nabla \eta_\alpha \quad , \tag{A-1}$$

where η_α is the plasma density of charged-particle species α (in this case, barium ions and electrons).

A low-β plasma with density gradients is confined in a magnetic field by diamagnetic drifts that result in $\vec{v} \times \vec{B}$ forces that balance pressure gradients arising from the variation in density. The diamagnetic drift is a direct result of density gradient and particle cyclotron motion interplay. The diamagnetic drift is given by

$$v_{D\alpha} = \frac{\varepsilon_\alpha}{2\Omega_\alpha} \langle v_{\perp\alpha}^2 \rangle \quad , \tag{A-2}$$

where Ω_α is the cyclotron frequency of species α, and $\langle v_{\perp}^2{}_\alpha \rangle$ is the average velocity of species α perpendicular to the magnetic field. Equation (A-2) shows that the diamagnetic drift velocity may be greatly enhanced by a peaked

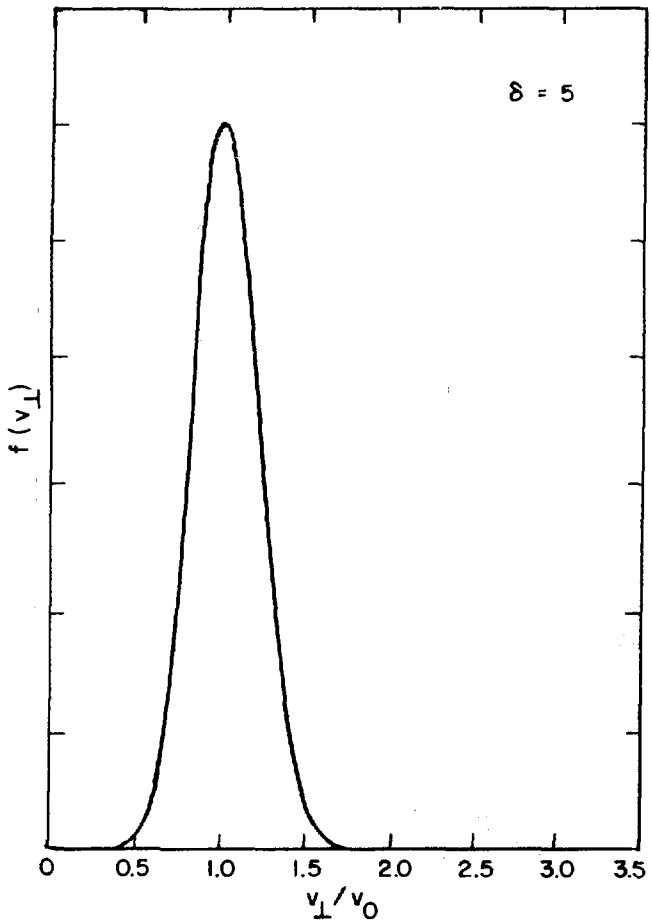

Fig. A-1
Peaked velocity distribution for $\delta = 5$, scaled in terms of the peak velocity, v_0.

perpendicular velocity distribution over a Maxwellian velocity distribution of similar temperature.

The peaked velocity distribution of our model is shown in Fig. A-1 and given by the relation

$$f(v_\perp) = \frac{\delta^2}{\sqrt{2\pi}\, v_0^2 A(\delta)}\, v_\perp \exp - \frac{(v_\perp - v_0)^2}{2v_T^2} \quad , \qquad \text{(A-3)}$$

where we have introduced three more parameters of the DCLC theory: v_0, the characteristic velocity of the peak; v_T, the rms velocity spread of the peak; and δ, the ratio of v_0 to v_T. The parameter $A(\delta)$ is a normalization parameter given by

$$A(\delta) = \frac{\pi}{2}(1 + \delta^2)[1 + \exp(\frac{\delta}{1.3})] + \delta \exp(-\frac{\delta^2}{2}) \quad . \qquad \text{(A-4)}$$

The low-β plasma supports a large variety of electrostatic waves that are always present at a low energy density, characteristic of thermal fluctuations. The various dispersion relationships that relate the frequency, ω; the wave number, κ; and the damping decrement, γ strongly depend on the plasma composition and geometry. Electrostatic waves that propagate parallel to the diamagnetic drifts $v_{D\alpha}$ and approximately satisfy the resonance condition $\omega - \vec{\kappa}\vec{v}_{D\alpha} = 0$ will absorb energy from the drift motion. As this energy is absorbed, the waves grow in amplitude, leading to an enhanced level of charge density fluctuations. Simultaneously, the diamagnetic drift velocity must decrease, leading to a cross-magnetic-field reconfiguration of the plasma. The determination of the readjustment of drift velocities, cross-field reconfiguration, and eventual wave amplitude saturation and convection requires a complete solution of the nonlinear kinetic equations in a complex geometry. It is not possible to obtain such a solution generally, even with high-speed computing techniques. This is why we need experiments like Aguila.

The linearized first-order equations for the DCLC predict the frequency and wave number regime of the most unstable waves for various selections of ε, v_0, v_T, δ, and Ω_i. The wavelength $\lambda_{max} = 2\pi/K_{max}$, where K_{max} is the wavenumber associated with the most unstable wave at ω_{max} and γ_{max}, is assumed to be the characteristic scale of the initial prompt striations. We introduce one other parameter that proves to be a useful length scale in this problem, that is ρ_0, the gyroradius of a barium ion with velocity v_0:

$$\rho_o \equiv \frac{v_o}{\Omega_i} . \qquad \text{(A-5)}$$

Table A-I summarizes the various DCLC parameters.

Figure A-2 shows the relationship of γ_{max} and δ for a particular value ε, chosen because it characterizes the three plasma clouds to be produced during Aguila.

As indicated, the linear theory does not contain any parameters that will truly predict the onset of striations, so we have developed two parameters from ad hoc physical arguments. (The linear parameters will only predict when conditions are correct for the initiation of instability.) If the wave spectrum saturates at too low an energy level due to an insufficient source of free energy, or if wave energy convects too rapidly out of the interaction region, striations will not develop. We have defined the free energy ε_f and the convection loss rate, τ_k. ε_f is the total energy in particle motion perpendicular to the magnetic field minus the effective perpendicular thermal energy:

TABLE A-I

DCLC PARAMETERS

$\omega \equiv$ frequency of flute mode electrostatic waves

$\kappa \equiv$ wavenumber of electrostatic waves

$\gamma \equiv$ exponential growth rate of wave amplitude

$\varepsilon \equiv$ density scale length of barium cloud

$v_o \equiv$ characteristic velocity of the perpendicular velocity distribution

$v_T \equiv$ rms velocity width of the perpendicular velocity distribution

$\phi \equiv v_o/v_T$

$\rho_o \equiv$ ion gyroradius of barium ion at velocity v_o

$\Omega_i \equiv$ barium gyrofrequency

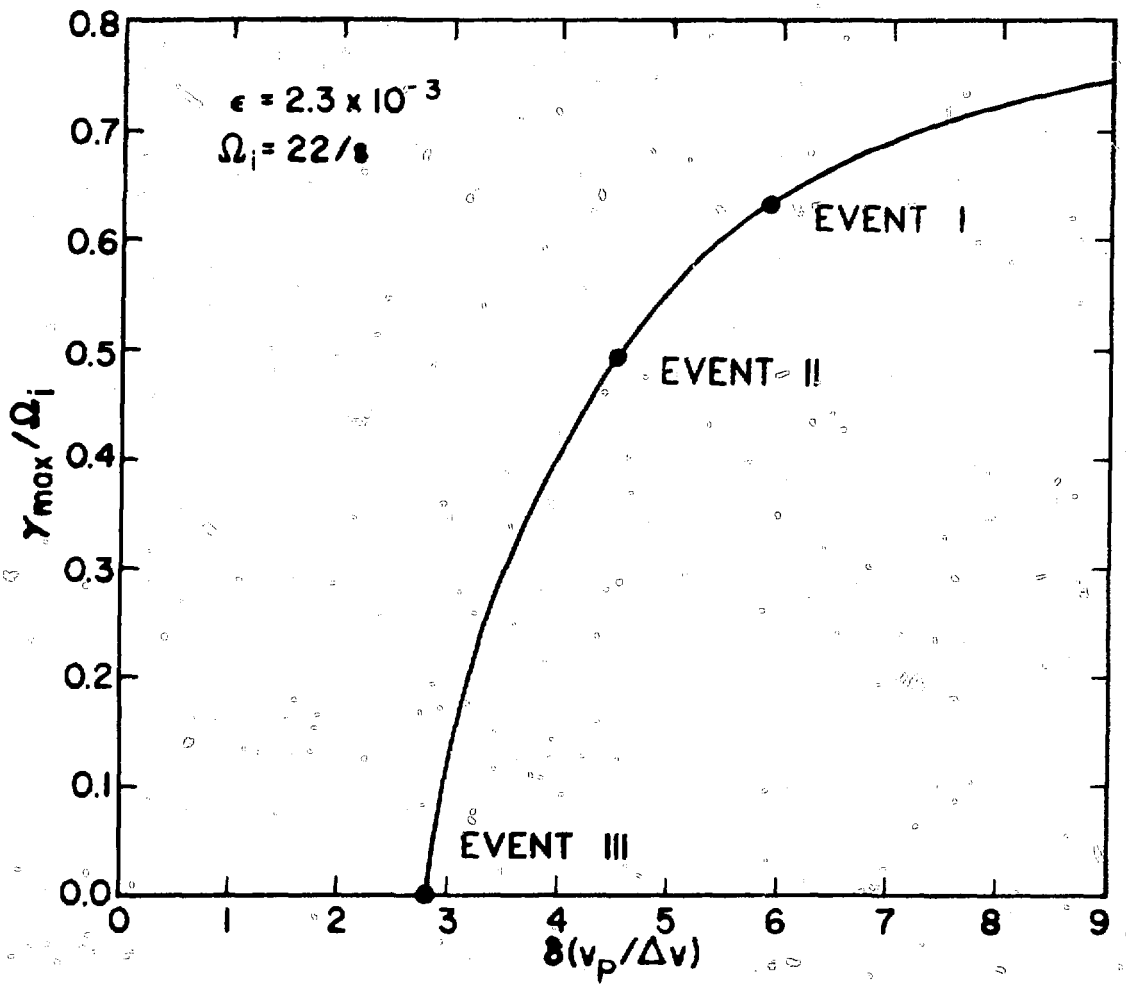

Fig. A-2
Growth rate at the point of maximum instability versus δ.

$$\varepsilon_i = \frac{1}{2} nm_B \langle v_\perp^2 \rangle - \frac{1}{2} nm_B \langle v_T^2 \rangle \quad . \qquad \text{(A-6)}$$

Taking ε_k to be the spectral energy density of electrostatic waves at wavenumber k, we define the rate of loss of ε_k out of the system by

$$\frac{d\varepsilon_k}{dt} = - \varepsilon_k / \tau_k \quad , \qquad \text{(A-7)}$$

with $(1/\tau_k) \sim (v_{gk}/L)$, where v_{gk} is the group velocity of a wave at wavenumber k and L is a characteristic size of the system perpendicular to the magnetic field. Equation (A-7) simply states that energy is carried out of the system at the group velocity in the time required to traverse the system.

The electrostatic waves that grow in amplitude and eventually cause the restructuring of the plasma density are readily absorbed by electrons in the high-energy tail of the Maxwellian distribution. Because of the small number of these electrons, they do not seriously interfere with the instability development, but they do lead to an excellant indirect diagnostic of the level of spectral energy density attained by the electrostatic waves. The electrons in the enhanced suprathermal tail of the velocity distribution will, through collisions, excite the various molecular and atomic species that form the background ionosphere. Above 300 km, the dominant species is atomic oxygen with the ground state transitions $^3P \rightarrow {}^1D(2.0\ eV)$ and $^3P \rightarrow {}^1S(4.2\ eV)$. The $^1S \rightarrow {}^1D$ transition is at 557.7 nm and the $^1D \rightarrow {}^3P$ is at 630.0 nm. The amount and extent of 630.0 nm and 557.7 nm will be a measure of the intensity of electrostatic waves and should give us a measure of the wave convection as well.

CHARACTERISTICS OF THE THREE RELEASES DURING AGUILA

Here we will explain how we estimated the various parameters characterizing the three barium releases in terms of the DCLC instability. Our estimates can only be made in an order-of-magnitude manner because the injection process is very complex, involving photoionization, magnetic trapping, adiabatic motion of the trapped ions, and eventual electrodynamic interactions of the plasma.

Spatial Extent and Gradient Scale Sizes

The spatial extent of the barium plasma is determined by interaction of the photoionization of barium atoms and rapid expansion of the neutral cloud. Assuming that, when created, a barium ion immediately becomes trapped in the magnetic field, we are led to the conclusion that the greatest ion density exists where the cloud is initially injected; the neutral density falls off very rapidly as the cloud expands into 4π steradians. Because the

neutral barium is essentially collisionless, it will travel until it is photoionized. This conclusion is complicated by the free motion of the trapped ion along the magnetic field and away from the region of the ion's creation. Figure A-3 is a compilation of empirical data on barium injections with 1-km/s characteristic injection velocities. Above 350 km, the half width of the cloud is essentially the 1-km/s injection velocity times the 20-s photoionization time of the barium neutrals. We compare this with a simple analytical model of the expansion; the results are shown in Fig. A-4 for dimensions perpendicular to the magnetic field. Using a model suggested by Haerendel, et al,[4] take $N_I(r,t)$ to be the density of ions, N_{BO} the total number of barium atoms, τ the photoionization time of barium neutrals, and $f(v)$ the initial velocity distribution of neutrals, and ignore parallel motion away from the

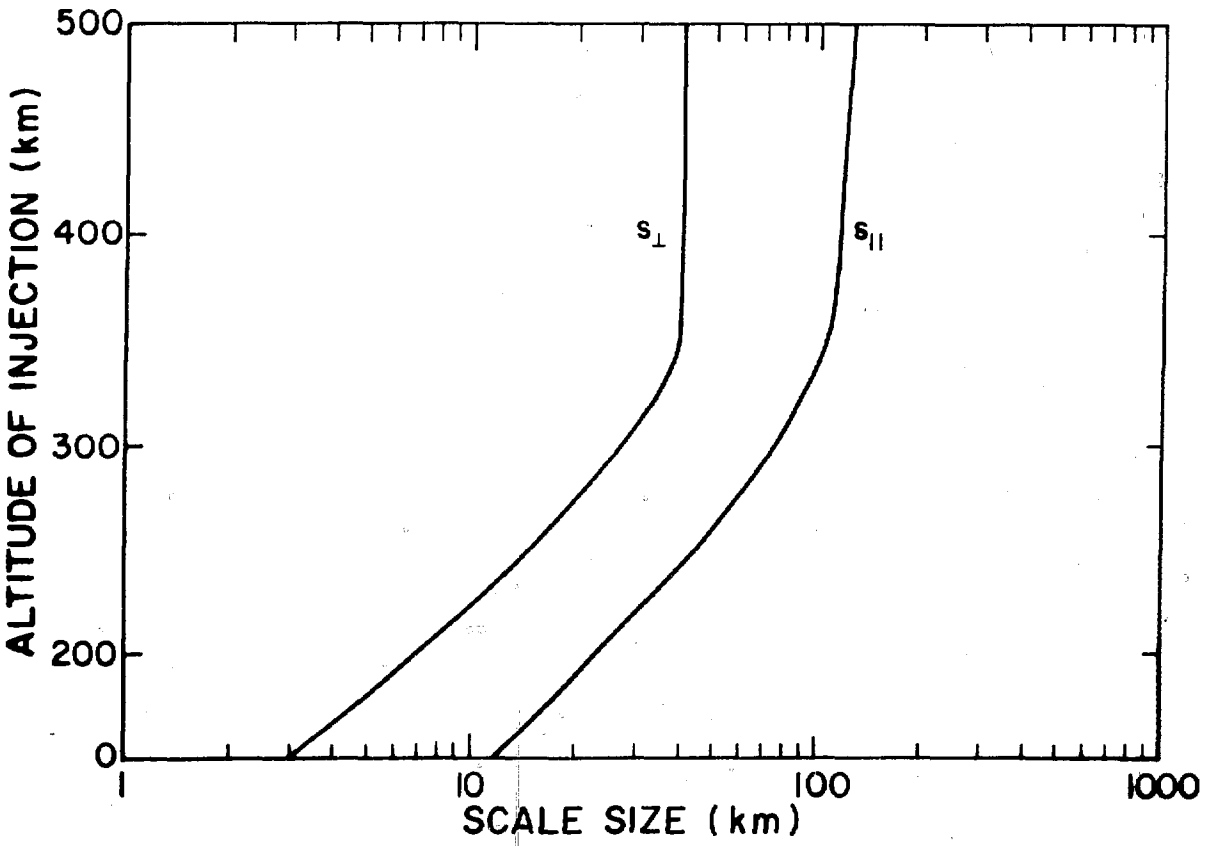

Fig. A-3
Transverse and perpendicular scale sizes for barium injections as a function of injection altitude.

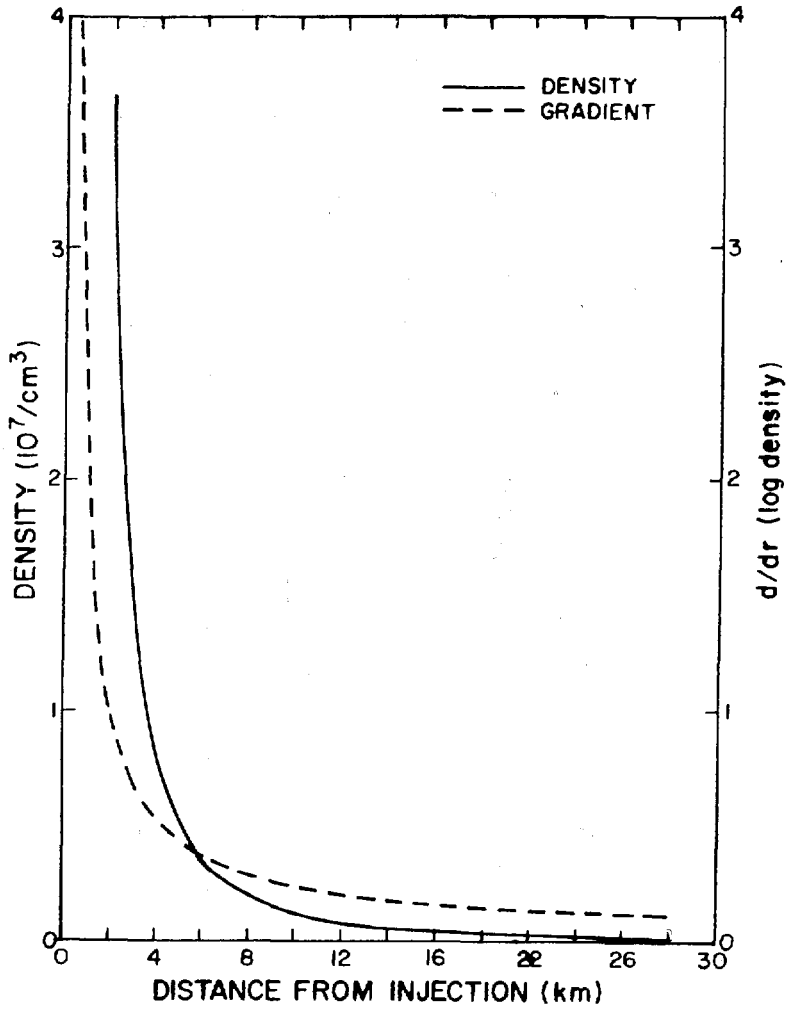

Fig. A-4
Simple analytical model of injection ignoring parallel-to-B motion of ions.

point of ionization, then the barium ion density at position r away from the injection and time t after injection is

$$N_I(r,t) = \frac{N_{BO}}{\tau} \int_0^t \frac{e^{-t/\tau}}{t^3} f(v = \frac{r}{t}) dt \quad . \qquad \text{(A-8)}$$

Figure A-4 is the result of numerically integrating Eq. (A-8) for the distribution function [Eq. (A-3)], using parameters characteristic of a spherically symmetric injection. This model suggests a half-width of about 3 km, which is drastically different from the 20 km of Fig. A-3. Combining the intuition

afforded by Eq. (A-3) and the data of Fig. A-3, we have adopted the following ad hoc model. We will assume that the ions are distributed along the magnetic field with an e-folding length given by $L = (v_0/2)t$ and across the magnetic field with an e-folding length $L_\perp = v_0\tau$. This leads to

$$N(r,z,t) = \frac{N_{BO}(1 - e^{-t/\tau})\, e^{-\frac{2z}{v_0 t}}\, e^{\frac{r}{v_0\tau}}}{.43\, v_0^3 t\tau^2 [1 - e^{Rt/\tau}(1 + t/\tau)]} \quad . \qquad \text{(A-9)}$$

We restrict t to less than 50 s, since the cloud expands parallel to the B-field to a length of about 150 km and then remains fixed. This yields the density scale ε,

$$\varepsilon = \frac{d\log N}{dr} = -\frac{1}{v_0\tau} \quad . \qquad \text{(A-10)}$$

We should point out that the predictions of Eq. (A-9) are in very good agreement with our monte carlo program PTRACE, which predicts the evolution of barium injections by following individual particle trajectories in a uniform magnetic field in the presence of a gravitational potential, ignoring plasma dynamics.

The initial injection velocity of the barium neutral atoms will be composed of the velocity of the expanding shell and the center of mass motion of the rocket at the time of injection. Table A-II lists the velocity of the rocket for the three injections shown in Fig. 1. $v_{\perp o}$ is the component perpendicular to the magnetic field. $v_{\parallel o}$ is the component parallel to the magnetic field, and θ is the angle between the field and the total velocity vector.

TABLE A-II

INJECTION PARAMETERS OF THE THREE EVENTS

	$v_{\perp o}$, km/s	$v_{\parallel o}$, km/s	θ_o, degrees
Event I	1.94	.75	111.69
Event II	1.25	.16	97.50
Event III	.38	.85	24.31

The gradient scale length will be evaluated by assuming that the v_o in Eq. (A-3) may be approximated by simply adding 1 km/s to the value of $v_{\perp o}$ shown in Table VI. The value of v_o in Eq. (A-3) will be the same. Table A-III lists the values of ε and ρ_o for the three events. An important deduction of Eq. (A-10) is that the quantity $\varepsilon\rho_o$ (the ratio of the ion gyroradius and the scale length in the plasma) is independent of v_o and is given by

$$\varepsilon\rho_o = \frac{1}{\Omega_i \tau_i} \quad . \tag{A-11}$$

The Linear Instability Regime

The critical DCLC instability parameter is the ratio of the peak velocity to the thermal velocity, δ. We assume that this thermal velocity is the same v_T that characterizes the original velocity spread in the neutral barium distribution, that is v_T = .5 km/s.

Using the values listed in Table A-III for $\varepsilon\rho_o$ and various values of δ, we solved the DCLC linear theory. Figure A-2 shows the maximum growth rate γ_{max} as a function of δ resulting from these calculations. The maximum value of γ occurs typically at a wavenumber

$$K_{max} = \frac{3.0}{\rho_o} \quad . \tag{A-12}$$

The parameters characterizing the three clouds are shown in Table A-IV.

TABLE A-III

INITIAL DCLC PARAMETERS OF THE THREE EVENTS

	v_o, km/s	ρ_o, km	ε, per km	$\varepsilon\rho_o$
Event I	2.94	.13	1.7×10^{-2}	2.3×10^{-3}
Event II	2.25	.10	2.2×10^{-2}	2.3×10^{-3}
Event III	1.38	.06	3.8×10^{-2}	2.3×10^{-3}

TABLE A-IV

DERIVED DCLC PARAMETER OF THE THREE EVENTS

	δ	γ_{max}, per s	λ_{max}, km
Event I	5.9	14	.27
Event II	4.5	11	.21
Event III	2.8	0	.13

Parameters for the Nonlinear Regime

The parameters ε_f, v_{gK}, and τ_K may also be calculated based on the data in Table A-III; these results are listed in Table A-V.

The value $\tau_K = 2.0 \times 10^7$ s tells us that wave convection may be ignored as a loss mechanism. There is also sufficient free energy in Event I to heat the entire electron population to a temperature > 2 eV, though this is highly unlikely.

TABLE A-V

NONLINEAR PARAMETERS OF THE THREE EVENTS

	ε_f, eV/particle	v_{gK}, km/s	τ_K, s
Event I	3.5	2.9×10^{-6}	2.0×10^7
Event II	1.8	2.3×10^{-6}	2.0×10^7
Event III	.9	1.4×10^{-6}	2.0×10^7

REFERENCES

1. D. Adamson, C. C. Fricke, S. A. T. Long, W. F. Landon, and D. L. Ridge, "Preliminary Analysis of NASA-Optical Data Obtained in Barium Ion Cloud Experiment of September 21, 1971," J.Geophys. Res. 78(25), 5769 (1973).

2. Hal T. Baber, Jr., Kenneth H. Crumbly, and David Adamson, compilers, "Barium Releases at Altitudes between 200 and 1000 kilometers, a Joint Max-Planck-Institut/NASA Experiment," National Aeronautics and Space Administration report NASA SP-264 (1971).

3. K. W. Michel, "Fluorescence in Jets for Studying the Ionosphere and Magnetosphere," Acta Astronautica 1, 37 (1974).

4. G. Haerendal, R. Lust, and B. Meyer, "MPI Analysis of Observations," in Hal T. Baber, et al, "Barium Releases at Altitudes between 200 and 1000 kilometers, a Joint Max-Planck-Institut/NASA Experiment," National Aeronautics and Space Administration report NASA SP-264, p. 15 (1971).

5. J. R. Breedlove, Jr., and E. P. Marram, "Geometric and Radiometric Data Reduction for Secede II Events Plum and Spruce," EGG report EGG 1183-5006 (1 December 1971).

6. S. L. Ossakow, P. K. Chaturvedi, and J. B. Workman, "High-Altitude Limit of the Gradient Drift Instability," Naval Research Laboratory Memorandum Report 3639 (1977).

7. H. J. Volk and G. Haesendel, "Striations in Ionospheric Ion Clouds," J. Geophys. Res. 76, 4541 (1971).

8. M. B. Pongratz and R. A. Jeffries, "Event Buaro, A Barium Plasma Injection Exactly Perpendicular to the Geomagnetic Field," LASL Internal Memorandum (1976).

9. John H. Wolcott and Robert A. Jeffries, "Project STRESS Operations Plan," LASL, J-10 internal memorandum (January 25, 1977).

10. D. J. Simons and M. B. Pongratz, "Prompt Striation Mechanisms," LASL Internal Report (1979).

11. D. J. Simons, M. B. Pongratz, and S. P. Gary, "Prompt Striations in Ionospheric Barium Clouds due to a Velocity Space Instability," submitted to J. Geophys. Res. (1979).

☆U.S. Government Printing Office: 1979 677—013/190